JOM, Vol. 69, No. 1, 2017
DOI: 10.1007/s11837-016-2154-0

In Situ TEM Scratch Testing of Perpendicular Magnetic Recording Multilayers with a Novel MEMS Tribometer

ERIC D. HINTSALA,[1,2] DOUGLAS D. STAUFFER,[1] YUNJE OH,[1] and S.A. SYED ASIF[1]

1.—Hysitron, Incorporated, Eden Prairie, MN, USA. 2.—e-mail: ehintsala@hysitron.com

Utilizing a newly developed two-dimensional (2D) transducer designed for in situ transmission electron microscope (TEM) nanotribology, deformation mechanisms of a perpendicular magnetic recording film stack under scratch loading conditions were evaluated. These types of films are widely utilized in storage devices, and loss of data by grain reorientation in the recording layers is of interest. The observed deformation was characterized by a stick–slip mechanism, which was induced by a critical ratio of lateral to normal force regardless of normal force. At low applied normal forces, the diamond-like carbon (DLC) coating and asperities in the recording layer were removed during scratching, while, at higher applied forces, grain reorientation and debonding of the recording layer was observed. As the normal force and displacement were increased, work for stick–slip deformation and contact stress were found to increase based upon an Archard's Law analysis. These experiments also served as an initial case study demonstrating the capabilities of this new transducer.

INTRODUCTION

Nanoindentation-based in situ transmission electron microscope (TEM) studies, starting around 10 years ago, have already produced numerous insights into fundamental materials behavior through the study of nanoparticles,[1–4] nanowires,[5–7] nanopillars[8–10] and indentation of thinned bulk materials.[9–11] Though researchers can probe mechanical behavior with sub-μN force and sub-nm displacements, a cohesive understanding of nanomechanical behavior of materials requires exploration of a wider variable space, including the state of stress. The state of stress has been evolving from the first experiments utilizing compression testing[1–4,6,8–10] to tension experiments.[4,6,12] Comparatively, shearing experiments are less utilized, though this stress state is crucial for understanding of interface properties and wear mechanisms. For instance, significant effort has been made by researchers studying debonding of multilayers to produce film stacks at a 45° angle relative to the indenter tip to induce shear,[13] and production of specialized double-notched pillars.[14] Though tribological studies have been performed in situ TEM,[15–20] one limitation has been the inability to measure and apply both forces and displacements in two perpendicular axes simultaneously, which requires a "two-dimensional (2D)" transducer which is compact enough for in situ TEM. Such a transducer would provide significant benefit for existing research efforts, from fundamental atomic scale tribology studies[15–18] to wear mechanisms in films[19] and nanoparticles,[20] and material mixing under shear[21] while potentially enabling new types of experiments.

In order to provide the increased force and displacement resolution needed for in situ TEM studies, as compared to existing 2D transducers, a 2D micro-electro-mechanical system-based (MEMS) transducer was developed. This transducer possesses resolution < 1 μN for both normal and lateral direction forces and utilizes an electrostatically actuated comb drive for normal direction force generation and capacitive displacement measurements. A piezoelectric actuator is used to move the transducer laterally while maintaining a pre-defined normal direction force setpoint. The lateral force is measured by monitoring lateral tip displacement via differential capacitance change in comb

(Published online October 24, 2016)

drive, knowing the spring constant of the cantilever. Thus, forces and displacements can be measured or controlled on both axes. This MEMS-based tribometer opens numerous possibilities, including identifying material deformation mechanisms under friction, testing nanoscale film delamination and nanoscale structural bending, and performing subnanometer topography measurements.

Here, we present some of the first experiments performed using this newly developed 2D MEMS transducer. These experiments study the deformation of perpendicular magnetic recording (PMR) hard disc drive (HDD) film stacks under scratching conditions, which is of industrial consequence. During even minor collisions, data loss by the read head scratching the platter is a common failure mechanism.[22,23] It has often been attributed to plastic reorientation of grains in the orientation layer,[23] which diverts the magnetic moment normally perpendicular to the film plane into the film plane, thus becoming undetectable to the read head. These devices are highly optimized to extract maximum performance, for instance, only a thin diamond-like carbon (DLC) protective overcoat is utilized,[24] typically only 2–3 nm. In situ TEM nanomechanical testing provides visualization of the deformation processes and could one day be paired with larger quantities of ex situ scratch data to produce more accurate material behavior models.[25] Such developments would be necessary to drive further performance optimization, whether it be through new DLC coating recipes or modification of the functional device layers.

MATERIALS AND METHODS

The material utilized was a multi-layer PMR film stack deposited using proprietary manufacturing parameters onto a silicon wedge substrate (~100 nm in width, and several μm in height) by anonymous collaborators in the HDD industry. The wedge substrate elevates the material of interest, thereby preventing shadowing due to sample mistilt, while also defining the film thickness along the electron beam axis. The film stack is composed of several layers as shown in Fig. 1a. The top three layers of the film stack are the primary focus of this study as they are most exposed to damage. A 2–3-nm-thick DLC overcoat is on top, which protects two recording layers: a 5–6-nm-thick metallic orientation layer and an approximately 12-nm-thick metal oxide layer. The magnetic oxide layer is a nominally stoichiometric equivalent oxide to the metallic layer and they possess a shared columnar grain structure which terminates as rounded asperities at the DLC interface, with a grain size of 5–15 nm. This film structure deposited onto the silicon wedge substrate produces a rounded apex wedge structure. This was imaged using the SPM imaging mode of a Hysitron TI-950 Triboindenter, equipped with a Berkovich tip at a 1-μN setpoint and a 1-Hz scan speed, from which extracted line profiles were taken which were utilized for analysis in the "Results and Discussion" section.

In situ scratch testing was performed using a Hysitron PI-95 PicoIndenter operating inside an FEI F30 TEM. Bright field imaging conditions were utilized at 300 keV accelerating voltage. Videos were recorded using digital capture of the camera search mode at 15 fps. A focused ion beam prepared sharp wedge diamond probe of approximately 50 nm radius of curvature and 500 nm length was used. Scratch tests were performed in normal axis load control at loads of 1, 2, 5, 10 and 20 μN while simultaneously measuring the lateral force and normal displacement. Transverse motion was achieved using an open loop piezo actuation based upon voltage/motion calibrations and the resulting lateral displacements were corrected by direct measurement from the acquired in situ TEM videos. The combined specimen and tip geometry represents two perpendicular rounded wedges in sliding contact as shown in Fig. 1b. This configuration differs from ex situ nanoindentation-based scratch testing in that the material is not confined along the electron beam axis, which is necessary to achieve electron transparency in the TEM. Although traditional scratch analysis methods[26] cannot be utilized due to the change in specimen constraint, this configuration allows unparalleled visibility of deformation during scratch loading.

RESULTS AND DISCUSSION

Two different types of material deformation were observed as a function of the applied normal load. At low normal loads, 1, 2 and 5 μN, the asperities of the columnar grains were flattened. At high normal loads, 10 and 20 μN, the grains underwent irreversible plastic bending. For all applied normal loads, the DLC layer was observed to buckle in front of the advancing tip with little resistance, which is proposed to be an electron beam irradiation effect based upon our previous in situ TEM indentation work on the same material, which showed a significant disparity at low loads for contact pressure.[21] Such effects should be the focus of future experiments to accurately determine the protection offered by the DLC layer, but will not be discussed further here. Next, the low-load and high-load regimes will be examined in greater detail by highlighting an experiment exhibiting each behavior.

An example of a low normal force experiment, 2 μN, is shown in Fig. 2a. Here, it can be observed that the discrete lateral load drops correlate to rapid lateral tip motion. This mechanism is generally referred to as "stick–slip" motion, where the lateral force builds to a critical level, which triggers rapid lateral tip motion until it is stopped by material pile-up in front of the tip, as observed in the corresponding TEM micrographs in Fig. 2b, c, d

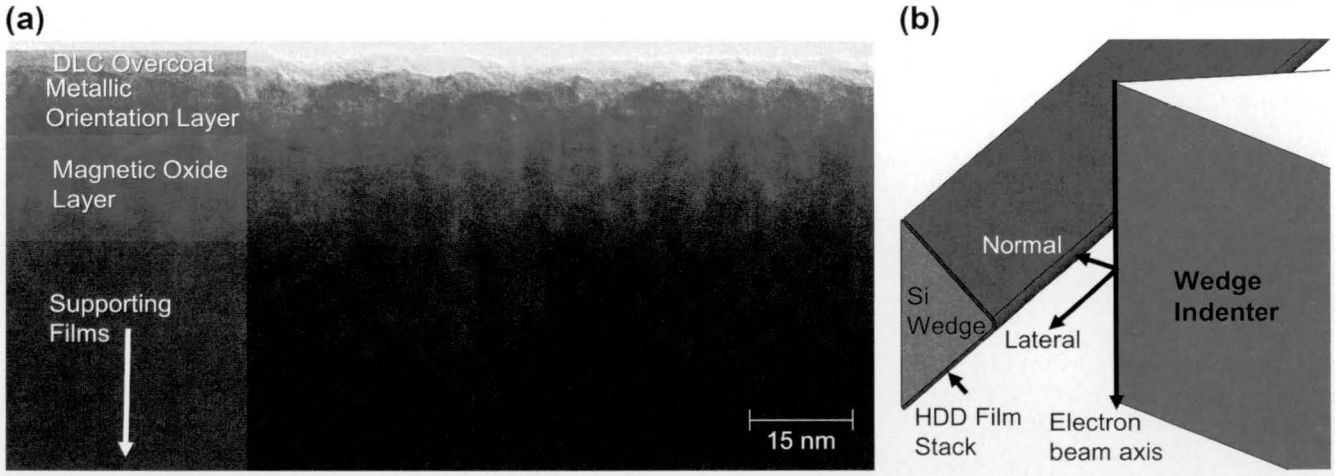

Fig. 1. (a) Bright field TEM micrograph of the HDD film stack, with markings to show the individual layers and (b) schematic showing the loading configuration of the deposited film stack by the wedge tip.

and e and Supplementary Video 1. The resulting deformation in the material during each cycle was asperity smoothing in the metallic orientation layer and buckling of the DLC layer in front of the tip, but no changes to the underlying grain structure could be detected. A high normal force scratch experiment, 20 μN, is shown in Fig. 3a. Discrete load drops in the transverse direction were not detected and the scratch load continues to increase throughout the experiment along with an increasing normal tip displacement indicative of plastic ploughing.[22] The observed deformation shows that the grains in the magnetic layer undergo reorientation, particularly obvious when observing a well-aligned grain near the upper portion of the video frame (Fig. 3b, c, d, e and f, Supplementary Movie 2). There was also evidence of debonding of the metallic orientation layer from the magnetic oxide below as the columnar grains in the compressive zone ahead of the tip can be observed to lose registry with each other as shown in Fig. 3g, h and i, which ultimately fully debonded during unloading. It is worth noting that the applied lateral displacement differs in these two tests as the lateral displacement is applied in open loop or voltage control. The actual lateral displacement applied is less for increasing material resistance as the normal force is increased, though lateral displacements can be made to match through adjusting the piezo actuation.

The magnitude of lateral load drops changed only slightly with depth, which was superimposed on an increasing base lateral force; see Fig. 4a for a comparison of lateral force versus time at the different normal loads applied. This is reflected by calculated friction coefficients, the ratio of the normal to lateral load, at the peak lateral force preceding a stick–slip event and at the base recovery point as shown in Fig. 4b. The peak friction coefficient was relatively constant, while the base value increased with depth. This also may explain why no stick–slip was observed in the 20-μN experiment, which did not reach the critical peak friction coefficient of 0.5 by the end of the applied lateral motion. The base friction coefficient appears to increase rapidly at ~7 nm depth. This might be explained by the tip penetrating past the asperities of the metallic orientation layer (which is a reasonable match for average measured asperity height of ~3.5 nm plus the DLC layer thickness of 2–3 nm) and corresponded to a change in deformation mechanism from asperity flattening to bending of the grains. This would occur as the deformed asperities can flow into the surrounding empty space without forcing reorientation of the rest of the columnar grains when the tip penetration is less than the asperity height.

Utilizing an Archard's Law[27] approach, similar to that performed by Jacobs et al.,[17,18] one can estimate a material hardness based upon the volume of removed material and lateral work during a stick–slip event. For this partially unconfined material, this may better be described instead as a critical contact stress rather than hardness. For this approach, utilizing the in situ TEM videos allows direct measurement of the projected area of the material removed. The film thickness was estimated using line-scan profiles from SPM imaging as described in the "Materials and Methods" section. An average specimen thickness, $\bar{t}$, was calculated over the normal displacement measured from the in situ video according to:

$$\bar{t} = \frac{1}{h}\int_0^h t(h)\mathrm{d}h \tag{1}$$

where t is the thickness and h is the normal displacement. Since this transducer allows for direct measurement of lateral force, one can calculate the work, W_L, per lateral jump as:

$$W_L = P_L \times \delta_L \tag{2}$$

where P_L is the peak lateral force and δ_L is the resulting lateral displacement. The volume of

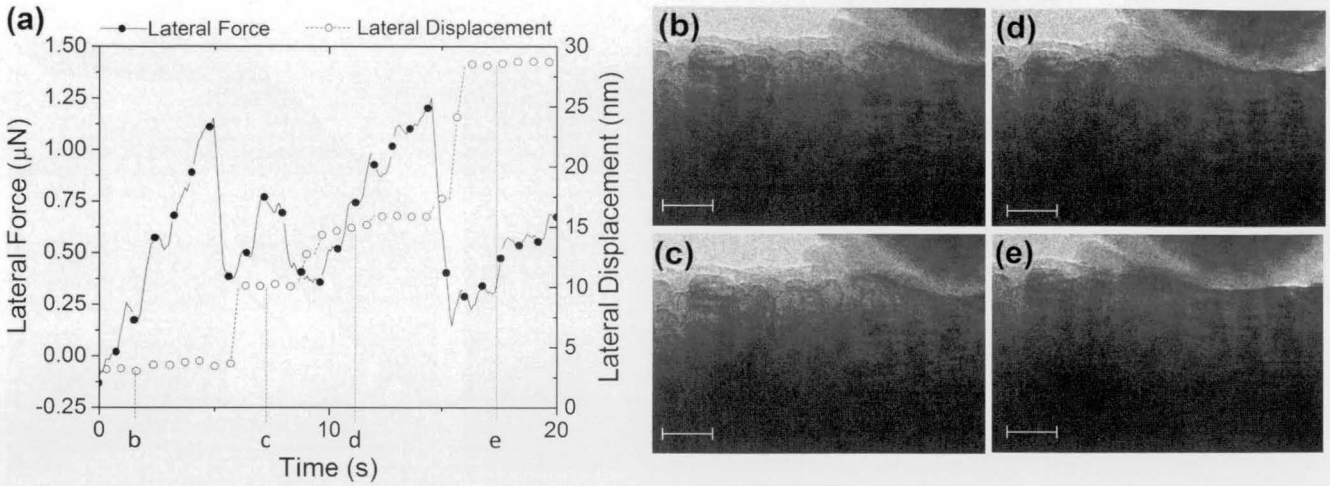

Fig. 2. A 2 μN normal force scratch experiment: (a) lateral load and displacement versus time and (b–g) corresponding TEM micrograph sequence taken from the in situ video. It can be observed that the DLC buckles and flows in front of the tip while the asperities of the metallic orientation layer are flattened. However, the grain structure does not undergo reorientation. Scale bar 10 nm.

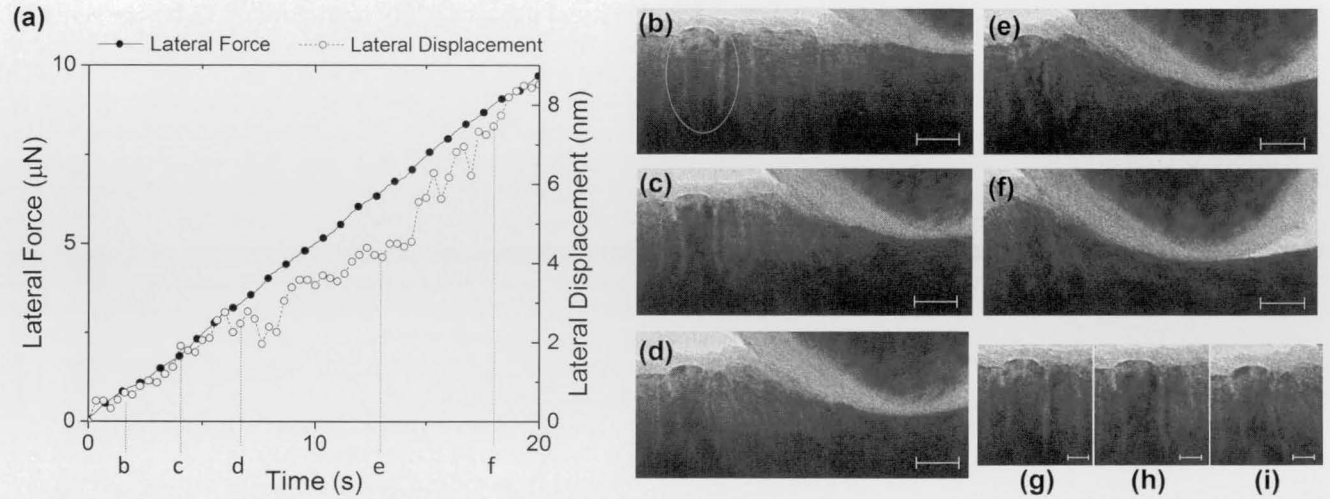

Fig. 3. A 20 μN normal force scratch experiment: (a) lateral load and displacement versus time and (b–f) corresponding TEM micrograph sequence taken from the in situ video. Scale bar 10 nm. The red circled grain in (b) was crystallographically aligned such that it displayed rapid contrast changes as the tip approached, signifying grain reorientation. This grain is enhanced in (g–i) where it also appears that debonding may have occurred between the metallic and oxide layer based upon the loss of registry across the grain boundary. Scale bar 5 nm.

material displaced versus the lateral work is plotted in Fig. 4c as a function of lateral work during stick–slip motion. The critical contact stress, $\sigma^*_{\text{contact}}$, for stick–slip motion is determined by dividing the work by the displaced volume as:

$$\sigma^*_{\text{contact}} = \frac{W_{\text{L}}}{V}. \tag{3}$$

The result is plotted in Fig. 4d, where it can be observed that the critical contact stress mimics the behavior of the base friction coefficient value in Fig. 4b, where it is relatively constant until ~7-nm depth, then increases drastically, suggesting a similar interpretation may be valid. Typically, Archard's Law shows a constant ratio between volume removal and work; however, since this is a multilayer system, the depth dependence of the contact stress and base friction coefficients make sense.

Thus, it appears that the change in deformation mechanism as a function of normal load observed from in situ TEM was correlated to changes in contact stress and the friction coefficients. Specifically, low depth deformation by asperity smoothing showed a low base friction coefficient and contact stress, which transitioned rapidly at a depth of ~7 nm to grain bending and increased base friction coefficient and contact stress. This was proposed to be correlated to the height of the film asperities, though it should be acknowledged that this mechanism is speculative at this point. To better address

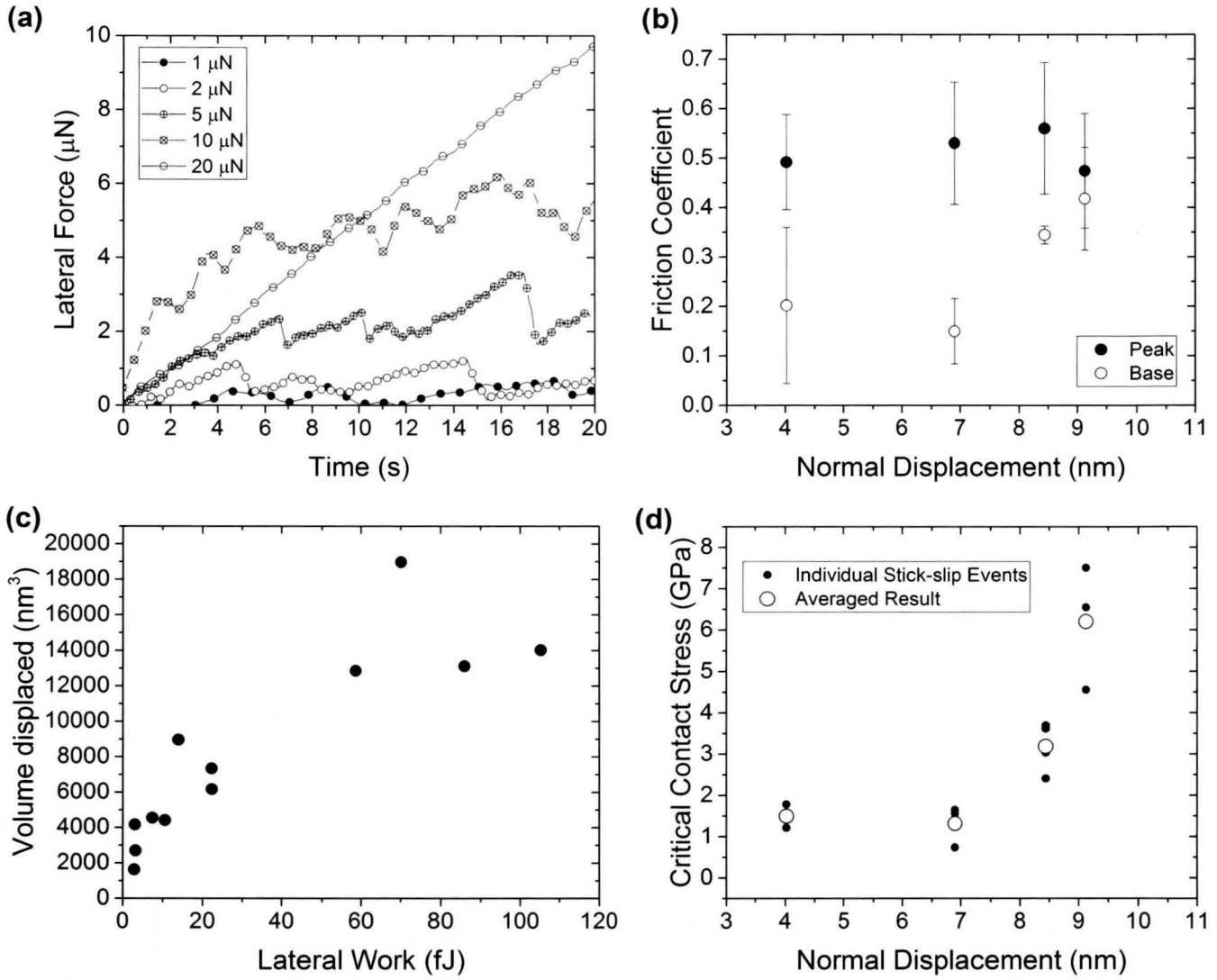

Fig. 4. (a) Comparison of the lateral force versus time for different normal loads on the HDD film stack, (b) analysis of the peak friction coefficient prior to a stick–slip event and the base friction coefficient immediately after as a function of normal displacement, (c) volume of material displaced as a function of lateral work, and (d) critical contact stress for stick–slip deformation as a function of normal displacement.

this, more rigorous analysis procedures that could extract the stress and strain distributions would be necessary and additionally allow analysis of the onset of the grain bending and debonding mechanisms as the tip advances under scratch loading conditions. This analysis could also be helpful for understanding the effects of the changed constraints for the thinned TEM specimens, especially if rigorous comparison to ex situ scratch on the same material were performed. Future experiments to evaluate the role of electron beam irradiation on the DLC layer deformation would also be valuable, as the performance of this protective layer is vital to optimal device performance. Lastly, direct confirmation of the change in magnetic moment of the sample after undergoing grain reorientation would be an insightful topic for future study.

CONCLUSION

The scratch loading of PMR HDD film stacks were a useful case study for demonstrating the capabilities of the new MEMS tribometer. The high force and displacement resolution along both the normal and lateral axes allowed depth-sensitive scratch properties on a complex multilayer system composed of individual layers only a few nm thick to be measured. This case study also demonstrated a variety of deformation behavior that can be explored with in situ TEM under scratch loading of films including buckling, asperity smoothing, grain bending and debonding. In addition, the in situ TEM configuration allows unparalleled visibility of the material deformation behavior and is useful as a correlative technique for determining deformation mechanisms. A critical friction coefficient was

identified for inducing stick–slip motion, along with a sudden increase in critical contact stress for stick–slip corresponding to a change in deformation mechanism from smoothing of asperities in the metallic orientation layer to grain bending.

ACKNOWLEDGEMENTS

The authors would like to acknowledge their anonymous collaborators in the hard disc drive industry for providing the samples with which this work was done.

ELECTRONIC SUPPLEMENTARY MATERIAL

The online version of this article (doi:10.1007/s11837-016-2154-0) contains supplementary material, which is available to authorized users.

REFERENCES

1. Z.W. Shan, G. Adesso, A. Cabot, M.P. Sherburne, S.A.S. Asif, O.L. Warren, D.C. Chrzan, A.M. Minor, and A.P. Alivisatos, *Nat. Mater.* 7, 947 (2008).
2. C.E. Carlton and P.J. Ferreira, *Micron* 43, 1134 (2012).
3. I. Issa, J. Amodeo, J. Réthoré, L. Joly-Pottuz, C. Esnouf, J. Morthomas, M. Perez, J. Chevalier, and K. Masenelli-Varlot, *Acta Mater.* 86, 295 (2015).
4. A.J. Wagner, E.D. Hintsala, P. Kumar, W.W. Gerberich, and K.A. Mkhoyan, *Acta Mater.* 100, 256 (2015).
5. Y. Lu, J. Song, J.Y. Huang, and J. Lou, *Adv. Funct. Mater.* 21, 3982 (2011).
6. B. Chen, J. Wang, Q. Gao, Y. Chen, X. Liao, C. Lu, H.H. Tan, Y.W. Mai, J. Zou, S.P. Ringer, and H. Gao, *Nano Lett.* 13, 4369 (2013).
7. H. Idrissi, C. Bollinger, F. Boioli, D. Schryvers, and P. Cordier, *Sci. Adv.* 2, E1501671 (2016).
8. D. Kiener and A.M. Minor, *Acta Mater.* 59, 1328 (2011).
9. Y. Kim, S. Lee, J.B. Jeon, Y.J. Kim, B.J. Lee, S.H. Oh, and S.M. Han, *Scr. Mater.* 107, 5 (2015).
10. A.M. Minor, J.W. Morris Jr, and E.A. Stach, *Appl. Phys. Lett.* 79, 1625 (2001).
11. M.S. Bobji, J.B. Pethica, and B.J. Inkson, *J. Mater. Res.* 20, 2726 (2005).
12. H.D. Espinosa, B.C. Prorok, and B. Peng, *J. Mech. Phys. Sol.* 52, 667 (2004).
13. N. Li, N.A. Mara, J. Wang, P. Dickerson, J.Y. Huang, and A. Misra, *Scr. Mater.* 67, 479 (2012).
14. C. Mayer, N. Li, N. Mara, and N. Chawla, *Mater. Sci. Eng. A* 621, 229 (2015).
15. S. Fujisawa and T. Kizuka, *Tribol. Lett.* 15, 163 (2003).
16. A.P. Merkle and L.D. Marks, *Wear* 265, 1864 (2008).
17. T.D. Jacobs and R.W. Carpick, *Nat. Nanotechnol.* 8, 108 (2013).
18. T.D. Jacobs, J.A. Lefever, and R.W. Carpick, *Adv. Mater. Interfaces* 2, (2015)..
19. A.P. Merkle, A. Erdemir, O.L. Eryilmaz, J.A. Johnson, and L.D. Marks, *Carbon* 48, 587 (2010).
20. I. Lahouij, F. Dassenoy, L. de Knoop, J.M. Martin, and B. Vacher, *Tribol. Lett.* 42, 133 (2011).
21. Z.P. Luo, G.P. Zhang, and R. Schwaiger, *Scr. Mater.* 107, 67 (2015).
22. M. Suk and D. Jen, *IEEE Trans. Magn.* 34, 1711 (1998).
23. S.C. Lee, S.Y. Hong, N.Y. Kim, J. Ferber, X. Che, and B.D. Strom, *J. Tribol.* 131, 011904 (2009).
24. C. Donnet and A. Erdemir, eds., *Tribology of Diamond-Like Carbon Films: Fundamentals and Applications* (Berlin: Springer, 2007).
25. E.D. Hintsala, S.A.S. Asif, and D.D. Stauffer, *MRS Adv.* 1, 799 (2016).
26. P.J. Burnett and D.S. Rickerby, *Thin Solid Films* 157, 233 (1988).
27. J.F. Archard, *J. Appl. Phys.* 24, 981 (1953).